ADVANCED MATERIALS
www.advmat.de

Direct Imaging of Dopant and Impurity Distributions in 2D MoS_2

Se-Ho Kim, Joohyun Lim, Rajib Sahu, Olga Kasian, Leigh T. Stephenson, Christina Scheu, and Baptiste Gault**

Molybdenum disulfide (MoS_2) nanosheet is a two-dimensional (2D) material with high electron mobility and with high potential for applications in catalysis and electronics. MoS_2 nanosheets are synthesized using a one-pot wet-chemical synthesis route with and without Re doping. Atom probe tomography reveals that 3.8 at% Re is homogeneously distributed within the Re-doped sheets. Other impurities are also found integrated within the material: light elements including C, N, O, and Na, locally enriched up to 0.1 at%, as well as heavy elements such as V and W. Analysis of the nondoped sample reveals that the W and V likely originate from the Mo precursor. It is shown how wet-chemical synthesis results in an uncontrolled integration of species from the solution that can affect the material's activity. The results of this work are expected to contribute to an improved understanding of the relationships linking composition to properties of 2D transition-metal dichalcogenide materials.

Molybdenum disulfide (MoS_2) is a semiconducting material; however, unlike bulk MoS_2 which has an indirect bandgap of 1.2 eV,[1] MoS_2 prepared as a 2D material has a direct bandgap of 1.8 eV[2] paired with a high electron mobility.[3] 2D MoS_2 shows advantageous properties for a wide array of applications in photo(electric)catalysis,[4,5] photoluminescence,[6] chemical sensors,[7] electronics for field-effect transistors,[8] and light harvesting devices.[9] Additionally, the oscillating piezoelectric voltage and current output[10] can be tuned by adjusting the number of stacked layers of MoS_2, indicating its potential application in powering nanodevices[11] and stretchable electronics.[12]

Control of the charge carrier concentration is a key to tune a material's electronic properties and its activity, and this is usually achieved by doping with the appropriate elements. For example, rhenium doping of MoS_2 (Re-MoS_2) nanosheets leads to the formation of a metallic 1T phase locally which is more conductive and catalytic active via 2D basal plane compared to the semiconducting 2H phase with edge limited catalytic activity.[13,14] However, the prospect of doped MoS_2 for high-performance electronics is still controversially debated.[15,16] One of the problems that hinders relating performance and doping stems from the challenge to measure the low-level concentration of p- or n-type dopants within 2D materials, which is necessary to understand their influence on the bandgap.[17] For example, Re is reported to be a n-type dopant but the local detection and quantification of Re within MoS_2 multilayer is difficult.[18,19] The presence of traces of spurious elements integrated within the structure during the synthesis could also detrimentally affect their properties. Identification and quantification of these impurities are however extremely challenging. Over the past few years, both computational and experimental approaches were used to study the influence of controlled levels of various dopants to adjust the bandgap for instance in MoS_2 nanostructures.[20,21]

Detailed chemical and compositional information at the near atomic-scale is required for explicit understanding of concentration-property relationships of both dopant and impurity. This is commonly gained through (scanning) transmission electron microscopy-energy-dispersive X-ray spectroscopy ((S)TEM-EDS) and X-ray photoelectron spectroscopy (XPS) to detect dopants and impurities.[22,23] Atom probe tomography (APT) represents an attractive alternative. APT is a burgeoning characterization technique allowing for mapping the elemental distribution in nanostructured materials with a unique combination of 3D capability, sub-nanometer spatial resolution, and ≈10–100 ppm level detection sensitivity for all elements irrespective of their mass.[24,25] APT shows great potential for nanomaterial characterization especially for dopant/impurity analysis.

Chemical vapor deposition (CVD) was used to deposit single 2D layer or only a few stacked layers, which can be used in electronic application.[26] Less well-controlled assemblies of 2D layers synthesized by wet-chemistry have been used for catalytic

S.-H. Kim, Dr. J. Lim, Dr. R. Sahu, Dr. O. Kasian, Dr. L. T. Stephenson, Prof. C. Scheu, Dr. B. Gault
Max-Planck-Institut für Eisenforschung GmbH
Max-Planck-Straße 1, Düsseldorf 40237, Germany
E-mail: j.lim@mpie.de; b.gault@mpie.de
Dr. O. Kasian
Helmholtz-Zentrum Berlin GmbH
Helmholtz-Institute Erlangen-Nürnberg
Berlin 14109, Germany
Dr. B. Gault
Department of Materials
Royal School of Mines
Imperial College
Prince Consort Road, London SW7 2BP, UK
The ORCID identification number(s) for the author(s) of this article can be found under https://doi.org/10.1002/adma.201907235.

DOI: 10.1002/adma.201907235

applications.[27–29] Here, we study self-assembled porous MoS_2 synthesized by a wet-chemical approach. This material exhibits a more complex morphology to characterize compared to a simple 2D sheet.

First, we studied the intentional doping of MoS_2 with Re by using APT. We also reveal unintentional doping by impurity elements present during the synthesis and originating from the metal-precursor or the solvent. Both heavy elements, such as V and W, and light elements such as C, N, and O were reported to act as electron acceptor (p-type dopant) and Na was reported to be an n-type dopant, up to a few atomic percent of all these elements are detected in the nanosheets. Underpinned by the challenge associated with measuring low quantities of these impurity elements, the influence of the presence of both dopant and impurity elements on the activity of the material have been too often neglected. This tends to restrict strategies to optimize the materials performance to being empirical rather than guided by physics or chemistry.

We first synthesized Re-doped MoS_2 nanosheets by using the one-pot wet-chemical method outlined by Xia et al.[19] Ammonium molybdate ($(NH_4)_6Mo_7O_{24}$) and thiourea (NH_2CSNH_2) precursors are dissolved along with ammonium perrhenate (NH_4ReO_4 for Re-doped MoS_2) in distilled water and heated at 200 °C for 20 h. The collected powder was then thoroughly rinsed with distilled water to remove excess impurities. The details are described in the Supporting Information.

Figure 1 shows transmission electron microscopy (TEM) image of the Re-doped MoS_2 nanosheets. We observe assemblies of 2D nanosheets, with ≈6.3 nm of stacked-layers of Re-doped MoS_2 as displayed in Figure 1a. (S)TEM-EDS (see Figure S1a in the Supporting Information) shows that Mo, S, and Re are apparently rather homogeneously distributed within the 2D assembled nanosheets. The details on peaks in EDS spectrum is described in Figure S1b (Supporting Information). The introduced Re induces locally the formation of the 1T phase in 2H phase of MoS_2 as shown in top view of high-resolution TEM images (Figure 1b,c).

In order to map the distribution of Re in 3D and to verify the presence of impurity elements in the Re-MoS_2 sheets, we performed APT. We used co-electrodeposition of a Ni-film to

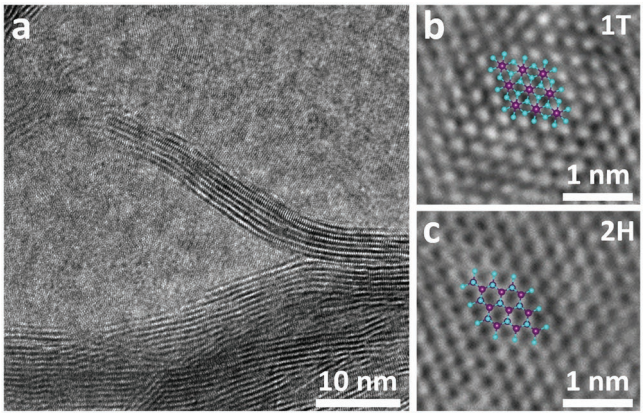

Figure 1. a–c) TEM images of Re-MoS_2 showing assembled morphology at a low magnification (a), and local phases of 1T (b) and 2H (c) at a high magnification (purple and cyan dots represent Mo and S atoms).

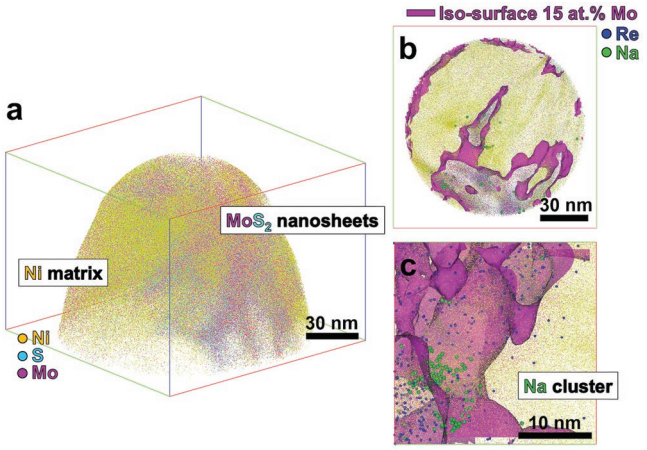

Figure 2. a) 3D atom map of Re-MoS_2 nanosheets embedded in Ni. b) 10 nm thin slice viewed along the *z*-axis and c) cubic region of interest ($25 \times 25 \times 25$ nm^3) sectioned from (a). The purple iso-composition surface with a threshold value of 15 at% Mo delineates the assembled MoS_2 nanosheets. The yellow, cyan, purple, blue, and green dots mark the reconstructed positions of Ni, S, Mo, Re, and Na atoms, respectively.

embed freestanding Re-MoS_2 nanosheets, applying the method described in ref. [30], so as to enable the preparation of a sharp specimens (<100 nm at the apex). A similar approach had previously been used for nanoparticles,[31–41] but never for 2D materials.

Scanning electron microscopy images obtained from the surface of the Ni/Re-MoS_2 co-electroplated sample are displayed in Figure S2a,b (Supporting Information). Following cross-sectional focused-ion beam milling (FIB), regions with a dark contrast appear in the micrographs in Figure S2c,d (Supporting Information). These regions are ascribed to assemblies of Re-MoS_2 nanosheets encapsulated in the Ni matrix, and, importantly, no noticeable voids can be detected. Site-specific APT specimen preparation was performed near one of these regions using the protocol outlined in ref. [42]. Experimental results from the Re-MoS_2 APT measurement are presented in Figure S3 (Supporting Information).

Figure 2a shows a reconstructed 3D atom map of the Re-MoS_2 nanosheets (Mo: purple, S: cyan) embedded in the Ni matrix (yellow). An iso-composition surface with a threshold of 15 at% for Mo highlights the interface between the MoS_2 nanosheets and the Ni matrix within a 10 nm thin slice viewed along the *z*-axis shows, as displayed in Figure 2b. The Re dopant atoms (in blue) clearly are partition into the nanosheets. As expected, Re-related peaks were not found in the Ni/MoS_2 by APT (see Figure S4 in the Supporting Information) indicating that Re only originates from the Re precursor.

A cuboidal region of interest of the Re-MoS_2 region viewed along the *z*-axis from the acquired 3D atom map (Figure 2c) reveals that Na atoms are distributed along the MoS_2 nanosheets. Na is not detected in the electroplated Ni (see Figure S5 in the Supporting Information). Therefore, Na atoms are stemmed from the Mo precursor reagent ($(NH_4)_6Mo_7O_{24}$, Sigma Aldrich) as it contains 0.01 wt% of Na by the chemical specification sheet. Across the nanosheets, ≈0.1 at% of Na is detected and segregated within Re-MoS_2, forming clusters of ≈4–5 nm in size (see Table S1 in the Supporting Information).

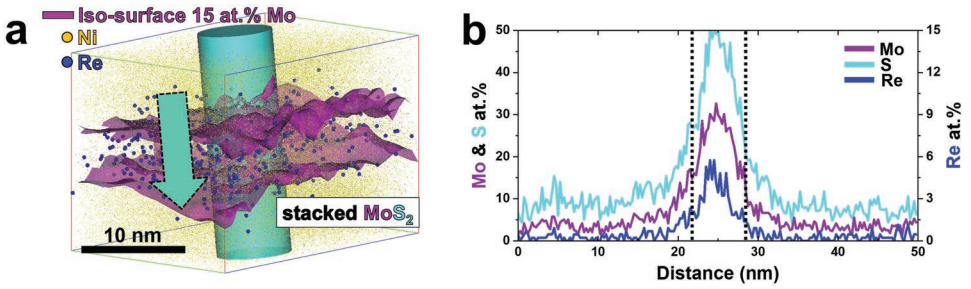

Figure 3. a) 3D atom map of one stacked Re-MoS_2 nanosheets with iso-concentration value of Mo at 15 at% (purple). The yellow and blue dots represent the reconstructed Ni and Re atoms, respectively. b) 1D compositional profile across Re-MoS_2 nanosheets.

From the density functional theory (DFT) calculations, Na doping was reported to enhance charge transfer of the MoS_2 by donating electrons causing, i.e., n-type doping.[43,44] Na is shown here incorporated within the nanosheets, and this is also rationalized by the excellent intercalation ability of MoS_2 for alkali ions with a high capacity and stability reported for metal-ion batteries.[45] Furthermore, it has been reported that Na atoms are detected in exfoliated-geological and CVD-grown MoS_2 nanosheets[46] as well as CVD-grown WS_2 nanosheets.[47]

Besides undesired impurity such as Na, unexpected heavy elements of V and W are also detected in both Re-doped and nondoped MoS_2 nanosheets. Detailed mass spectra are presented in Figure S6 (Supporting Information). Strong peaks are detected for $^{51}V^+$ and all the natural isotopes of W^+ (see Table S2 in the Supporting Information). These elements are not found in the APT mass spectrum of the Ni matrix, i.e., where no Re-MoS_2 are detected (see Figure S5 in the Supporting Information), whereas they are also observed in the nondoped MoS_2 (see Figure S7 in the Supporting Information). V and W hence most likely come from the Mo precursor. According to the chemical specification sheet of the Mo precursor reagent ($(NH_4)_6Mo_7O_{24}$, Sigma Aldrich), it contains 0.001 wt% of "heavy metals" impurities. Despite significant attention to extract high-purity Mo, the separation of Mo from V and W is reported to be very difficult, since they have similar chemical properties[48–50] and are known impurities within Mo.[51] Therefore, V and W likely remain alongside Mo.

We performed X-ray photoelectron spectroscopy (XPS) on Re-MoS_2 samples to look for trace amounts of V, W, and Na (see Figure S9 in the Supporting Information). No impurities other than C, N, and O were found, which is due to the detection limit of XPS. Although a noisy peak ≈37 eV might be assigned to W 4f, the signal-to-noise ratio around the peak is too small because of the low W concentration. Addou et al. used inductively coupled plasma mass spectrometry (ICP-MS) and time-of-flight mass spectrometry (TOF-MS) on CVD-grown MoS_2 nanosheets and found V and W within MoS_2.[46] Likewise, they did not detect these elements by XPS.

DFT calculation for $V_{0.08}Mo_{0.92}S_2$ showed increased electronic properties, with, in particular, a 40 time increase in the in-plane conductivity and 20 times higher carrier concentration than MoS_2. This change in properties led to higher catalytic activity for the hydrogen evolution reaction.[52] However, the bulk atomic compositions of V and W in the Re-MoS_2 are only 419 and 206 ppm, respectively. The W is expected to occupy the Mo-sites in the hexagonal parent structure of MoS_2[53,54] and V doping is also considered as intralayer doping in MoS_2.[54] The bandgap of the semiconducting phase (2H structure) of VS_2 (1.87 eV)[55] and WS_2 (1.91 eV)[56] are similar to that of MoS_2 (1.78 eV).[56] Moreover, VS_2, WS_2, and MoS_2 lattice constants are 0.317, 0.318, and 0.318 nm, respectively, so very close to each other.[57] The presence of V and W in such low concentration here could have only a limited effect on the electronic properties of MoS_2, yet this would need to be confirmed by complementary local electronic- and catalytic property measurements in comparison to materials with better control over the incorporation of such impurities.

Figure 3a shows an isolated stacked-layer of Re-MoS_2 extracted from a larger reconstructed dataset containing multiple nanosheets, evidenced by a set of iso-composition surfaces encompassing regions containing over 15 at% Mo. The composition of the Re-doped nanosheets is extracted from a 1D profile calculated within a cylindrical region of interest positioned perpendicular to the nanosheets, as plotted in Figure 3b. The Mo composition at the core of the MoS_2 nanosheets value is ≈30 at%. The thickness of the layer is approximately 7 nm, which agreed with TEM observations of the Re-MoS_2 nanosheet layers. Re atoms, shown in blue, are homogeneously distributed throughout the MoS_2 nanosheets. This is supported by a nearest-neighbor analysis reported in Figure S8 (Supporting Information). The composition of Re reaches 5.8 at% in the center of the sheet and is on average 3.8 at% within the nanosheets, suggesting that one Re atom substitutes to every 7.9 Mo atoms. Re could affect the transition from 2H to 1T, as predicted by crystal field theory.[14,18,19] When Re atoms are present in the 2H-MoS_2 system, an additional electron from Re can be stabilized by the bonding orbital of 1T compared to the nonbonding orbital in 2H. Even though it was reported that the overall energy landscape favors the transition when the composition in Re is over 50 at%,[14] the presence of kinetically favored local phase transition is expected in the Re-MoS2 prepared using lower temperature as in the present work.[19]

The atomic concentration ratio of S to Mo in the Re-doped MoS_2 nanosheets are 1.7 which is lower than the expected stoichiometry of MoS_2. It has been reported that single-layer MoS_2 oxidizes under ambient condition[58] as S vacancies are formed through oxidation spontaneously followed by O substitution process.[59] Using DFT calculation, the enthalpies of each reaction step were calculated to be −0.49 eV for S vacancy formation and −0.39 eV for O saturation, which implies that the oxidation is hence thermodynamically favorable.[60] Moreover, it is well known that the surface of MoS_2 oxidizes naturally.[61,62] This

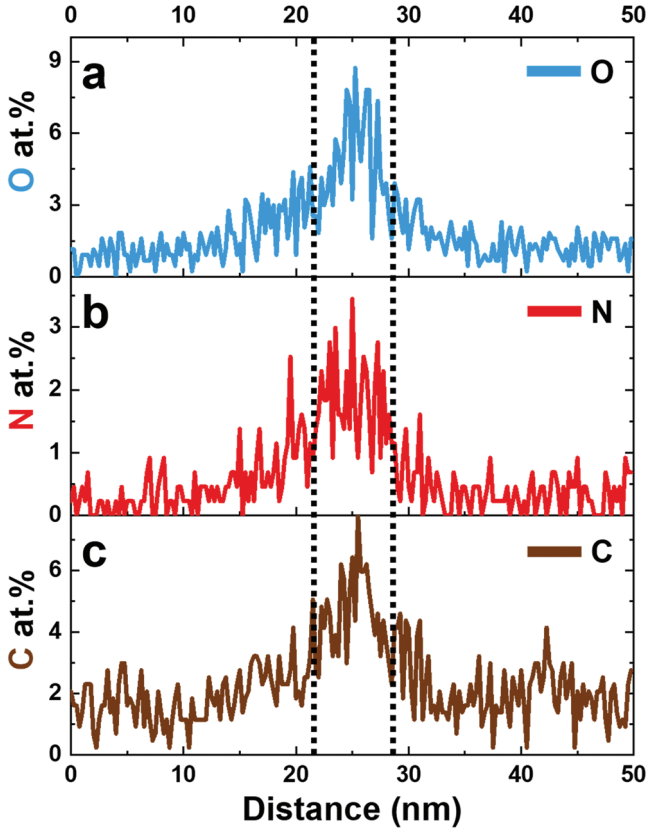

Figure 4. a–c) 1D atomic concentration profiles of O (a), N (b), and C (c) across the reconstructed Re-MoS_2 in Figure 3a.

reaction results in a complex molecular structure of $MoS_{(2-x)}O_x$.[63] Peaks pertaining to $MoSO^+$ molecular ions are detected (see Figure S3b in the Supporting Information) and the 1D profile across the reconstructed MoS_2 nanosheets clearly show that the presence of O is not limited to the surface but rather through the MoS_2 assemblies as shown in **Figure 4**a. As a result, the stoichiometric ratio of S + O to Mo gives 1.9. Some S vacancies are expected since S vacancies are reported to be the most abundant defects in MoS_2[64] and Re doping, which pushes the MoS_2 Fermi level close to its conduction band, could result in favorable formation of S vacancies.[65] Furthermore, it is also possible that some of the S is lost during field evaporation, as has been observed for some covalently bonded materials,[66] but the correlation histograms calculated here do not give indications of such specific losses as shown in Figure S10 (Supporting Information).

The enrichment in N and C in the Re-doped MoS_2 nanosheets are also evidenced in Figure 4b,c. N and C can either originate from the precursors of Mo ($(NH_4)_6Mo_7O_{24}$), Re (NH_3ReO_4), and S (NH_2CSNH_2) or be adsorbed from the atmosphere between synthesis and final preparation for analysis, and subsequently diffused inside MoS_2. They end up incorporated within the MoS_2 as well with average compositions of 2.4% and 6.4 at%, respectively. The incorporation of C in MoS_2 is reported to facilitate the transfer of the photogenerated electrons and holes that makes the photocatalytic reaction more efficient enhancing photocatalytic reaction[67] likewise the N incorporation improves the electronic conductivity of MoS_2 showing outstanding performance for hydrogen evolution reaction.[68] However, it was not possible to detect such elements locally at relatively low concentration with surface science spectroscopy. In contrast, our approach of using APT and TEM allows to obtain ppm-level chemistry information with high spatial resolution for 2D materials.

In conclusion, direct imaging of the as-synthesized Re-doped MoS_2 nanosheets is done using TEM and APT. The Re dopant is shown to have been incorporated within the MoS_2 structure, with an average composition of 3.8 at%, and we clearly observe other impurities from heavy (V, W) to light element (C, N, O, Na), with Na showing a tendency for clustering. Our results indicate that elements from the precursor were incorporated into the nanosheets during its synthesis. The chemistry of the MoS_2 synthesized using wet-chemical method is much more complex than expected and often reported. Controlling the synthesis environment is crucial to avoid contamination. We expect that our approach, amenable to other nanomaterials, will help understanding the role of dopant and impurity elements on the activity of MoS_2 nanosheets.

Experimental Section

Re-Doped and Nondoped MoS_2 Nanosheet Synthesis: 0.989 g of $(NH_4)_6Mo_7O_{24}{\cdot}4H_2O$ (Sigma-Aldrich (Germany), ACS reagent, 99.98% trace metals basis) and 2.284 g of NH_2CSNH_2 (Sigma-Aldrich (Germany), ACS reagent, ≥99.0%) were dissolved in 10 ml of distilled water along with or without 0.376 g of NH_4ReO_4 (Sigma-Aldrich, 99.999% trace metals basis) and a homogeneous transparent solution was prepared. Then, the solution was poured into a Teflon container placed in a stainless-steel autoclave and heated at a fixed temperature of 200 °C. After 20 h, the autoclave was cooled down to room temperature and the black powder was collected. Then the powder was repeatedly washed thrice with ethanol and distilled water for each centrifugation and re-dispersion steps. For MoS_2 materials, oxygen plasma cleaning for impurities removal of residuals could not be used since the O plasma induces substitutional oxidation of MoS_2 resulting $MoSO/MoO_3$ solid solution crystal.[60] Heat treatment in calcination method for removals could result MoC from as-synthesized MoS_2[69] and this surface cleaning method could not efficiently remove all C-based molecules.[70] Therefore, for removal of residuals, the water-washing treatment was chosen.[71] Finally, the rinsed powder was dried at room temperature.

Sample Preparation—Co-Electrodeposition Process: As-synthesized MoS_2 nanosheets were electrodeposited within Ni film for embedding nanoparticles according to Kim et al.[72] Nickel sulfate hexahyrdrate ($NiSO_4{\cdot}6H_2O$, Sigma-Aldrich (Germany)), and boric acid (H_3BO_3, Sigma-Aldrich (Germany)) were dissolved in distilled water. The nanosheets were then dispersed in as-prepared electrolyte solution and poured in a vertical cell for co-electrodeposition process. The vertical cell including a Cu substrate and a Pt-mesh counter electrode was used. A positive bias was applied to Pt electrode and electrodeposition of MoS_2 nanosheets and Ni were performed at constant current of –19 mA for 500 s.

TEM Analysis: TEM was performed to investigate morphology and crystal phase of Re-MoS_2 using 60–300 Titan Themis operated at 300 kV with a Cs corrector for the image forming lens. Chemical composition was analyzed using EDS in STEM mode (60–300 Titan Themis operated at 300 kV with a Cs corrector for the probe).

XPS Analysis: XPS measurements were performed (Quantera II, Physical Electronics, Chanhassen, MN, USA) applying a monochromatic Al Kα X-ray source (1486.6 eV) operating at 15 kV and 25 W. The binding energy scale was referenced to the C 1s signal at 285.0 eV. Analysis of the spectra was carried out with the Casa XPS (http://www.casaxps.com/) software.

APT Analysis: Needle-shaped APT specimens were prepared from MoS_2/Ni composite film using focused ion beam (FIB) (Helios 600) according to Thompson et al.[42] CAMECA LEAP 5000 XS system in pulsed laser mode at a specimen temperature of 50 K was used for nanosheets APT analysis. A laser pulse energy of 80 pJ and a pulse frequency of 125 kHz were set. Data reconstruction was done using the Imago visualization and analysis system (IVAS) 3.8.4 developed by CAMECA instruments. The standard voltage protocol was used for all data-set reconstruction.[73]

Supporting Information

Supporting Information is available from the Wiley Online Library or from the author.

Acknowledgements

S.-H.K., L.T.S., and B.G. acknowledge the financial support from the ERC-CoG-SHINE-771602. J.L. acknowledges the financial support from the Alexander von Humboldt Foundation.

Conflict of Interest

The authors declare no conflict of interest.

Author Contributions

S.-H.K. and J.L. contributed equally to this work. S.-H.K. performed the atom probe specimen preparation and atom probe analysis, with support from L.T.S. and B.G. S.-H.K. and B.G. drafted the manuscript. J.L. performed the synthesis. J.L. and R.S. performed the TEM with support from C.S. O.K. performed the XPS. All authors then contributed and have given approval to the final version of the manuscript.

Keywords

2D nanomaterials, atom probe tomography, molybdenum disulfide

Received: November 4, 2019
Revised: December 12, 2019
Published online: January 13, 2020

[1] C. B. Roxlo, R. R. Chianelli, H. W. Deckman, A. F. Ruppert, P. P. Wong, *J. Vac. Sci. Technol., A* **1987**, *5*, 555.
[2] K. F. Mak, C. Lee, J. Hone, J. Shan, T. F. Heinz, *Phys. Rev. Lett.* **2010**, *105*, 136805.
[3] W. Wu, D. De, S.-C. Chang, Y. Wang, H. Peng, J. Bao, S.-S. Pei, *Appl. Phys. Lett.* **2013**, *102*, 142106.
[4] Y. Li, Y.-L. Li, C. M. Araujo, W. Luo, R. Ahuja, *Catal. Sci. Technol.* **2013**, *3*, 2214.
[5] F. M. Pesci, M. S. Sokolikova, C. Grotta, P. C. Sherrell, F. Reale, K. Sharda, N. Ni, P. Palczynski, C. Mattevi, *ACS Catal.* **2017**, *7*, 4990.
[6] A. Splendiani, L. Sun, Y. Zhang, T. Li, J. Kim, C. Chim, G. Galli, F. Wang, *Nano Lett.* **2010**, *10*, 1271.
[7] F. K. Perkins, A. L. Friedman, E. Cobas, P. M. Campbell, G. G. Jernigan, B. T. Jonker, *Nano Lett.* **2013**, *13*, 668.
[8] A. Dankert, L. Langouche, M. V. Kamalakar, S. P. Dash, *ACS Nano* **2014**, *8*, 476.
[9] D. Lembke, A. Kis, *ACS Nano* **2012**, *6*, 10070.
[10] W. Wu, L. Wang, Y. Li, F. Zhang, L. Lin, S. Niu, D. Chenet, X. Zhang, Y. Hao, T. F. Heinz, J. Hone, Z. L. Wang, *Nature* **2014**, *514*, 470.
[11] J. Su, L. Feng, X. Zheng, C. Hu, H. Lu, Z. Liu, *ACS Appl. Mater. Interfaces* **2017**, *9*, 40940.
[12] P. Z. Hanakata, Z. Qi, D. K. Campbell, H. S. Park, *Nanoscale* **2016**, *8*, 458.
[13] R. Sahu, U. Bhat, N. M. Batra, H. Sharona, B. Vishal, S. Sarkar, S. Assa Aravindh, S. C. Peter, I. S. Roqan, P. M. F. J. Costa, R. Datta, *J. Appl. Phys.* **2017**, *121*, 105101.
[14] S.-Z. Yang, Y. Gong, P. Manchanda, Y.-Y. Zhang, G. Ye, S. Chen, L. Song, S. T. Pantelides, P. M. Ajayan, M. F. Chisholm, W. Zhou, *Adv. Mater.* **2018**, *30*, 1803477.
[15] G. Akhgar, O. Klochan, L. H. Willems van Beveren, M. T. Edmonds, F. Maier, B. J. Spencer, J. C. McCallum, L. Ley, A. R. Hamilton, C. I. Pakes, *Nano Lett.* **2016**, *16*, 3768.
[16] F. Schwierz, J. Pezoldt, R. Granzner, *Nanoscale* **2015**, *7*, 8261.
[17] K. Dolui, I. Rungger, C. Das Pemmaraju, S. Sanvito, *Phys. Rev. B* **2013**, *88*, 75420.
[18] T. Hallam, S. Monaghan, F. Gity, L. Ansari, M. Schmidt, C. Downing, C. P. Cullen, V. Nicolosi, P. K. Hurley, G. S. Duesberg, *Appl. Phys. Lett.* **2017**, *111*, 203101.
[19] B. Xia, P. Liu, Y. Liu, D. Gao, D. Xue, J. Ding, *Appl. Phys. Lett.* **2018**, *113*, 13101.
[20] H. Zhang, W. Zhou, Z. Yang, S. Wu, F. Ouyang, H. Xu, *Mater. Res. Express* **2017**, *4*, 126301.
[21] J. Suh, T.-E. Park, D.-Y. Lin, D. Fu, J. Park, H. J. Jung, Y. Chen, C. Ko, C. Jang, Y. Sun, R. Sinclair, J. Chang, S. Tongay, J. Wu, *Nano Lett.* **2014**, *14*, 6976.
[22] G. Deokar, D. Vignaud, R. Arenal, P. Louette, J.-F. Colomer, *Nanotechnology* **2016**, *27*, 75604.
[23] A. W. Robertson, Y.-C. Lin, S. Wang, H. Sawada, C. S. Allen, Q. Chen, S. Lee, G.-D. Lee, J. Lee, S. Han, E. Yoon, A. I. Kirkland, H. Kim, K. Suenaga, J. H. Warner, *ACS Nano* **2016**, *10*, 10227.
[24] M. K. Miller, E. a Kenik, *Microsc. Microanal.* **2004**, *10*, 336.
[25] D. Larson, T. Prosa, T. Kelly, *Local Electrode Atom Probe Tomography: A User's Guide*, Springer, New York, **2013**.
[26] W. Zhang, J.-K. Huang, C.-H. Chen, Y.-H. Chang, Y.-J. Cheng, L.-J. Li, *Adv. Mater.* **2013**, *25*, 3456.
[27] C. Altavilla, M. Sarno, P. Ciambelli, *Chem. Mater.* **2011**, *23*, 3879.
[28] C. Tan, H. Zhang, *Nat. Commun.* **2015**, *6*, 7873.
[29] X. Zhang, Z. Lai, C. Tan, H. Zhang, *Angew. Chem., Int. Ed.* **2016**, *55*, 8816.
[30] S. H. Kim, P. W. Kang, O. O. Park, J. B. Seol, J. P. Ahn, J. Y. Lee, P. P. Choi, *Ultramicroscopy* **2018**, *190*, 30.
[31] K. Tedsree, T. Li, S. Jones, C. W. A. Chan, K. M. K. Yu, P. A. J. Bagot, E. A. Marquis, G. D. W. Smith, S. C. E. Tsang, *Nat. Nanotechnol.* **2011**, *6*, 302.
[32] E. Folcke, R. Lardé, J. M. Le Breton, M. Gruber, F. Vurpillot, J. E. Shield, X. Rui, M. M. Patterson, *J. Alloys Compd.* **2012**, *517*, 40.
[33] S.-H. Kim, J. Y. Lee, J.-P. Ahn, P.-P. Choi, *Microsc. Microanal.* **2019**, *25*, 438.
[34] T. Li, P. A. J. Bagot, E. A. Marquis, S. C. E. Tsang, G. D. W. Smith, *J. Phys. Chem. C* **2012**, *116*, 17633.
[35] P. Felfer, P. Benndorf, A. Masters, T. Maschmeyer, J. M. Cairney, *Angew. Chem., Int. Ed.* **2014**, *53*, 11190.
[36] P. R. Heck, F. J. Stadermann, D. Isheim, O. Auciello, T. L. Daulton, A. M. Davis, J. W. Elam, C. Floss, J. Hiller, D. J. Larson, J. B. Lewis, A. Mane, M. J. Pellin, M. R. Savina, D. N. Seidman, T. Stephan, *Meteorit. Planet. Sci.* **2014**, *49*, 453.
[37] T. Li, P. A. J. Bagot, E. Christian, B. R. C. Theobald, J. D. B. Sharman, D. Ozkaya, M. P. Moody, S. C. E. Tsang, G. D. W. Smith, *ACS Catal.* **2014**, *4*, 695.

[38] D. J. Larson, A. D. Giddings, Y. Wu, M. A. Verheijen, T. J. Prosa, F. Roozeboom, K. P. Rice, W. M. M. Kessels, B. P. Geiser, T. F. Kelly, *Ultramicroscopy* **2015**, *159*, 420.
[39] P. Felfer, T. Li, K. Eder, H. Galinski, A. P. Magyar, D. C. Bell, G. D. W. Smith, N. Kruse, S. P. Ringer, J. M. Cairney, *Ultramicroscopy* **2015**, *159*, 413.
[40] D. E. Perea, J. Liu, J. Bartrand, Q. Dicken, S. T. Thevuthasan, N. D. Browning, J. E. Evans, *Sci. Rep.* **2016**, *6*, 22321.
[41] B. G. Chae, J. H. Lee, S. Park, E. Lee, C. M. Kwak, M. Jafari, Y. K. Jeong, C. G. Park, J. B. Seol, *ACS Nano* **2018**, *12*, 12109.
[42] K. Thompson, D. Lawrence, D. J. Larson, J. D. Olson, T. F. Kelly, B. Gorman, *Ultramicroscopy* **2007**, *107*, 131.
[43] T. Komesu, D. Le, X. Zhang, Q. Ma, E. F. Schwier, Y. Kojima, M. Zheng, H. Iwasawa, K. Shimada, M. Taniguchi, L. Bartels, T. S. Rahman, P. A. Dowben, *Appl. Phys. Lett.* **2014**, *105*, 241602.
[44] T. Komesu, D. Le, I. Tanabe, E. F. Schwier, Y. Kojima, M. Zheng, K. Taguchi, K. Miyamoto, T. Okuda, H. Iwasawa, K. Shimada, T. S. Rahman, P. A. Dowben, *J. Phys.: Condens. Matter* **2017**, *29*, 285501.
[45] T. Yang, J. Liang, I. Sultana, M. M. Rahman, M. J. Monteiro, Y. (Ian) Chen, Z. Shao, S. R. P. Silva, J. Liu, *J. Mater. Chem. A* **2018**, *6*, 8280.
[46] R. Addou, S. McDonnell, D. Barrera, Z. Guo, A. Azcatl, J. Wang, H. Zhu, C. L. Hinkle, M. Quevedo-Lopez, H. N. Alshareef, L. Colombo, J. W. P. Hsu, R. M. Wallace, *ACS Nano* **2015**, *9*, 9124.
[47] J. Zhou, J. Lin, X. Huang, Y. Zhou, Y. Chen, J. Xia, H. Wang, Y. Xie, H. Yu, J. Lei, D. Wu, F. Liu, Q. Fu, Q. Zeng, C.-H. Hsu, C. Yang, L. Lu, T. Yu, Z. Shen, H. Lin, B. I. Yakobson, Q. Liu, K. Suenaga, G. Liu, Z. Liu, *Nature* **2018**, *556*, 355.
[48] D. R. Hay, R. K. Skogerboe, E. Scala, *J. Less-Common Met.* **1968**, *15*, 121.
[49] H.-I. Kim, K.-W. Lee, D. Mishra, K.-M. Yi, J.-H. Hong, M.-K. Jun, H.-K. Park, *J. Ind. Eng. Chem.* **2015**, *21*, 1265.
[50] H. T. Truong, T. H. Nguyen, M. S. Lee, *Hydrometallurgy* **2017**, *171*, 298.
[51] T. H. Nguyen, M. S. Lee, *Ind. Eng. Chem. Res.* **2014**, *53*, 8608.
[52] X. Sun, J. Dai, Y. Guo, C. Wu, F. Hu, J. Zhao, X. Zeng, Y. Xie, *Nanoscale* **2014**, *6*, 8359.
[53] S. Wang, A. Robertson, J. H. Warner, *Chem. Soc. Rev.* **2018**, *47*, 6764.
[54] A. A. Tedstone, D. J. Lewis, P. O'Brien, *Chem. Mater.* **2016**, *28*, 1965.
[55] M. Kan, B. Wang, Y. H. Lee, Q. Sun, *Nano Res.* **2015**, *8*, 1348.
[56] Z. Hu, S. Zhang, Y.-N. Zhang, D. Wang, H. Zeng, L.-M. Liu, *Phys. Chem. Chem. Phys.* **2015**, *17*, 1099.
[57] J. Du, C. Xia, W. Xiong, T. Wang, Y. Jia, J. Li, *Nanoscale* **2017**, *9*, 17585.
[58] J. Gao, B. Li, J. Tan, P. Chow, T.-M. Lu, N. Koratkar, *ACS Nano* **2016**, *10*, 2628.
[59] R. C. Longo, R. Addou, S. KC, J.-Y. Noh, C. M. Smyth, D. Barrera, C. Zhang, J. W. P. Hsu, R. M. Wallace, K. Cho, *2D Mater.* **2017**, *4*, 25050.
[60] J. Pető,T. Ollár, P. Vancsó, Z. I. Popov, G. Z. Magda, G. Dobrik, C. Hwang, P. B. Sorokin, L. Tapasztó, *Nat. Chem.* **2018**, *10*, 1246.
[61] R. Ionescu, A. George, I. Ruiz, Z. Favors, Z. Mutlu, C. Liu, K. Ahmed, R. Wu, J. S. Jeong, L. Zavala, K. A. Mkhoyan, M. Ozkan, C. S. Ozkan, *Chem. Commun.* **2014**, *50*, 11226.
[62] S. KC, R. C. Longo, R. M. Wallace, K. Cho, *J. Appl. Phys.* **2015**, *117*, 135301.
[63] G. Colas, A. Saulot, D. Philippon, Y. Berthier, D. Leonard, *Thin Solid Films* **2015**, *588*, 67.
[64] L. Feng, J. Su, S. Chen, Z. Liu, *Mater. Chem. Phys.* **2014**, *148*, 5.
[65] H.-P. Komsa, A. V Krasheninnikov, *Phys. Rev. B* **2015**, *91*, 125304.
[66] B. Gault, D. W. Saxey, M. W. Ashton, S. B. Sinnott, A. N. Chiaramonti, M. P. Moody, D. K. Schreiber, *New J. Phys.* **2016**, *18*, 33031.
[67] Z. Hai, J. Du, M. K. Akbari, C. Xue, H. Xu, S. Zhuiykov, *Ionics* **2017**, *23*, 1921.
[68] W. Zhou, D. Hou, Y. Sang, S. Yao, J. Zhou, G. Li, L. Li, H. Liu, S. Chen, *J. Mater. Chem. A* **2014**, *2*, 11358.
[69] J. Jeon, Y. Park, S. Choi, J. Lee, S. S. Lim, B. H. Lee, Y. J. Song, J. H. Cho, Y. H. Jang, S. Lee, *ACS Nano* **2018**, *12*, 338.
[70] P. Mohapatra, S. Shaw, D. Mendivelso-Perez, J. M. Bobbitt, T. F. Silva, F. Naab, B. Yuan, X. Tian, E. A. Smith, L. Cademartiri, *Nat. Commun.* **2017**, *8*, 2038.
[71] J. A. Lopez-Sanchez, N. Dimitratos, C. Hammond, G. L. Brett, L. Kesavan, S. White, P. Miedziak, R. Tiruvalam, R. L. Jenkins, A. F. Carley, D. Knight, C. J. Kiely, G. J. Hutchings, *Nat. Chem.* **2011**, *3*, 551.
[72] S.-H. Kim, P. W. Kang, O. O. Park, J.-B. Seol, J.-P. Ahn, J. Y. Lee, P.-P. Choi, *Ultramicroscopy* **2018**, *190*, 30.
[73] P. Bas, A. Bostel, B. Deconihout, D. Blavette, *Appl. Surf. Sci.* **1995**, *87–88*, 298.